Eur. Phys. J. Appl. Phys. **53**, 30101 (2011)
DOI: 10.1051/epjap/2010100318

THE EUROPEAN PHYSICAL JOURNAL APPLIED PHYSICS

Regular Article

# Structural, elastic, electronic, optical and thermal properties of cubic perovskite $CsCdF_3$ under pressure effect

B. Ghebouli[1,a], M.A. Ghebouli[2], and M. Fatmi[3]

[1] Département de Physique, Faculté des Sciences, Université de Sétif, 19000 Sétif, Algeria
[2] Département de Physique, Centre Universitaire, 34000 Bordj Bou-Arréridj, Algeria
[3] Laboratoire de Physique et Mécanique des Matériaux Métalliques (LP3M), Université de Sétif, 19000 Sétif, Algeria

Received: 17 August 2010 / Received in final form: 12 December 2010 / Accepted: 17 December 2010
Published online: 22 February 2011 – 

**Abstract.** We have investigated the structural, elastic, electronic, optical and thermal properties of an insulator perovskite $CsCdF_3$ using the pseudo-potential plane wave (PP-PW) scheme in the frame of generalized gradient approximation (GGA) and local density approximation (LDA). The computed lattice parameter and bulk modulus agree reasonably with experimental and previous theoretical works. We find that the cubic Pm-3m crystal symmetry persists throughout the pressure range studied. The anisotropy in $CsCdF_3$ crystal is strong, while, by analyzing the ratio between the bulk and shear moduli, we conclude that $CsCdF_3$ is ductile material. The calculations reveal that $CsCdF_3$ is an indirect-gap insulator under ambient conditions, with the gap increasing under pressure. Also, we present the results of the densities of states and charge densities. The static dielectric constant and static refractive index are proportional to the fundamental indirect band gap Γ-R. The thermal effect on the volume, bulk modulus, heat capacities $C_V$ and $C_P$ and Debye temperature was predicted using the quasi-harmonic Debye model. To the author's knowledge, most of the studied properties are reported for the first time.

## 1 Introduction

The ternary fluorides with the perovskite crystal structure have been extensively investigated, because they have many potential applications due to their wide band gaps, optical properties [1,2], ferroelectricity [3], antiferromagnetism [4] and semiconductivity [5]. There are many kinds of perovskite-type fluorides, in particular, the Cs-based $CsXF_3$ (X = Ca, Sr, Cd and Hg) [6]. The application of $CsCdF_3$ in the field of luminescence has motivated several experimental and theoretical investigations of defect structures involving $3d$ transition-metal ions. Vaitheeswaran et al. investigated the crystal structure and elastic constants of $CsCdF_3$ using X-ray diffraction and theoretically at equilibrium [7]. This family of perovskites fluorides, $CsXF_3$ shows a larger Cs–F distance than the X–F one.

The preparation of perovskites $CsXF_3$ followed the procedure described in the literature [8]. CsF and $XF_2$ were first mixed and ground in a molar ratio of 1:1. The obtained powder was pressed into a pellet, closed in a gold tube, and then sealed in a silica tube under argon. The silica tube was annealed, followed by a slow cooling of the ampoule.

The optical properties of perovskites are anisotropic, show the phenomenon of birefringence and Their geometry is related to the chemical composition, temperature and pressure [9]. According to Lufaso and Woodward [10], a cubic perovskite can transform into other crystal structures. This perovskite fluoride not exhibit structural phase transition as function of temperature and pressure.

The use of first principles calculations offers one of the most powerful tools for carrying out theoretical studies of an important number of physical and chemical properties of the condensed matter with great accuracy [11,12]. In this work, we will contribute to the study of the perovskite fluoride $CsCdF_3$ by performing a first principles investigation of their structural, elastic, electronic, optical and thermal properties under pressure. The reason behind the variation of properties with pressure is the lattice constant, which varies under pressure and the structural phase transition. A number of basics properties of this compound are still unknown. To the best of our knowledge, there are no experimental or theoretical works exploring the thermal properties and the related elastic constants under pressure effect.

The letter is organized as follows: in Section 2, we briefly described the computational techniques used in this work. Results and discussions of our study will be presented in Section 3. Finally, conclusions and remarks are given in Section 4.

[a] e-mail: bghebouli@yahoo.fr

## 2 Computational method

The first-principles calculations were performed using the CASTEP code, in which the plane-wave pseudo-potential total energy method was used [13]. Interactions of electrons with ion cores were represented by the Vanderbilt-type ultrasoft pseudo-potential for Cs, Cd and F atoms [14]. The exchange-correlation potential was calculated within the local density approximation (LDA) developed by Ceperly and Alder [15] and parameterized by Perdew and Zunger [16] as well as the generalized gradient approximation (GGA) of Perdew et al. [17]. The plane-wave basis set cut-off was set as 350 eV for all cases. The special points sampling integration over the Brillouin zone was employed by using the Monkhorst-Pack method with an $8 \times 8 \times 8$ special $k$-point mesh [18]. These parameters were sufficient in leading to well converged total energy, geometrical configurations and elastic moduli. The structural parameters were determined using the Broyden-Fletcher-Goldfarb-Shanno (BFGS) minimization technique [19], with the following thresholds for converged structures, energy change per atom less than $5 \times 10^{-6}$ eV, residual force less than 0.01 eV/Å, stress below 0.03 GPa and the displacement of atoms during the geometry optimization less than 0.0005 Å.

The study of thermal effects was done within the quasi-harmonic Debye model implemented in the Gibbs program [20]. For a solid described by an energy-volume ($E$-$V$) relationship in the static approximations, the Gibbs program allows us to evaluate Debye temperature, to obtain the Gibbs free energy $G(V, P, T)$ and to minimize $G$ for deriving the thermal equation of state (EOS) $V(P, T)$. The detailed description of the quasi-harmonic Debye model was found in [20–24].

## 3 Results and discussions

### 3.1 Crystal structure

The cubic unit cell of $CsCdF_3$ contains one molecule with the Cs sitting at the origin (0, 0, 0), the Cd at the body center (0.5, 0.5, 0.5) and the three fluorine atoms at the face centers (0.5, 0.5, 0), (0.5, 0, 0.5) and (0, 0.5, 0.5). The calculated lattice parameter within GGA and LDA are summarized in Table 1. Also shown for comparison are the experimental and theoretical data reported by Moreira and Dias [25] and Jiang et al. [26]. The theoretical equilibrium lattice constant $a_0$, the bulk modulus $B_0$ and its pressure derivative $B'$ are determined by fitting the total energy versus the volume to the Murnaghan equation of state [27]. The lattice constant obtained within the LDA is 1.4% lower than the experimental value. A better theoretical description is also obtained with the LDA for $KMgF_3$ [28]. The LDA bulk modulus obtained from the present calculation agrees well with the experimental one cited in reference [7]. The computed lattice constant using GGA deviates from the experimental one within 1.8%.

**Table 1.** Calculated lattice constants $a_0$ (in Å), bulk modulus $B_0$ (in GPa) and its pressure derivative $B'$ for $CsCdF_3$ compound compared with the experiment and other theoretical calculations.

| | Present work | | Experiment | Other |
|---|---|---|---|---|
| | GGA (PBE) | LDA (CA-PZ) | | calculations |
| $a_0$ | 4.5558 | 4.4062 | [a] 4.47 | [a] 4.43, [b] 4.475 |
| $B_0$ | 53.6955 | 75.0457 | [a] 79 | [c] 53.3 |
| $B'$ | 4.92 | 4.979 | – | [c] 3.8 |

[a] [25], [b] [26], [c] [7].

**Table 2.** Calculated zero-pressure elastic constants ($C_{11}$, $C_{12}$ and $C_{44}$), bulk modulus $B$ (calculated from the elastic constants as $B = (C_{11} + 2C_{12})/3$) and anisotropy factor for $CsCdF_3$ compound.

| | $C_{11}$ | $C_{12}$ | $C_{44}$ | $B$ | $A$ |
|---|---|---|---|---|---|
| LDA | 136.48 | 44.12 | 21.78 | 74.91 | 0.47 |
| GGA | 96.62 | 35.36 | 20.53 | 50.238 | 0.67 |
| Exp | [a] $107.8 \pm 0.2$ | [a] $40.5 \pm 0.5$ | [a] $25 \pm 0.2$ | | [c] 0.74 |
| Other | | | | | |
| LDA | [c] 150.2 | [c] 27 | [c] 27.7 | | [c] 0.49 |
| GGA | [c] 105.8 | [c] 38.3 | [c] 27.5 | | [c] 0.7 |

[a] [25], [c] [7].

The obtained $B_0$ and $B'$ values are listed in Table 1. The bulk modulus is a measure of the crystal rigidity, thus a large compressibility is for high crystal rigidity.

### 3.2 Stability of $CsCdF_3$

The elastic constants of $CsCdF_3$ calculated within LDA and GGA are depicted in Table 2, where they are also compared to experimental results [29] as well as earlier calculations [7]. The LDA overestimates $C_{11}$ and $C_{12}$ and underestimates $C_{44}$ between 21, 8.2 and 14.7% compared to experiment values. The $C_{11}$ obtained within GGA is much closer to the experimental value; while, $C_{12}$ and $C_{44}$ values given by LDA are closer to the experimental ones. For $KMgF_3$, the elastic constants obtained within GGA are much closer to the experimental values than are the LDA results [28]. We can notice that all GGA elastic constants are within the experimental spread. Of course, the elastic constants also depend sensitively on the volume, and, therefore, the same argument as for the bulk modulus can be applied here. Using the calculated elastic constants, we calculated the anisotropy factor $A = 2C_{44}/(C_{11} - C_{12})$. For an isotropic crystal, $A$ is equal to 1, while any value smaller or larger than 1 indicates anisotropy. The magnitude of the deviation from 1 is a measure of the degree of elastic anisotropy possessed by the crystal. We find an $A = 0.47$ for LDA and $A = 0.67$ for GGA. The experimental value calculated from the elastic constants is 0.74 [7], which is strong within LDA compared to GGA. The anisotropy is strong within GGA compared to LDA, then the anisotropy factor is sensitive to exchange-correlation functional.

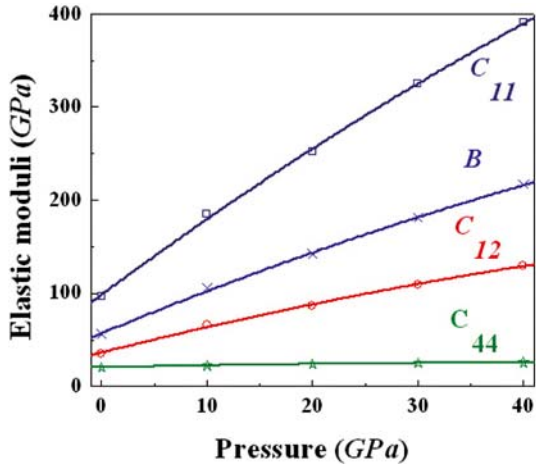


**Fig. 1.** (Color online) Elastic moduli $C_{11}$, $C_{12}$, $C_{44}$ and $B$ as a function of pressure.

A simple relationship, which empirically links the plastic properties of materials with their elastic moduli was proposed by Pugh [30]. The shear modulus $G$ represents the resistance to plastic deformation, while the bulk modulus $B$ represents the resistance to fracture. A high $B/G$ ratio is associated with ductility, whereas a low value corresponds to brittle nature. The critical value which separates ductile and brittle materials is around 1.75, i.e. if $B/G > 1.75$ the material behaves in a ductile manner; otherwise the material behaves in a brittle manner.

In the case of $CsCdF_3$ the calculated $B/G$ value is 2.53 within LDA and 2.08 within GGA, hence classifying this material as ductile. The consequence of ductility is the less sensitivity for thermal shocks, as the material can efficiently dissipate thermal stress via plastic deformations. Thus, a ductile solid can support large thermal shocks. Pettifor [31] suggested that the angular character of atomic bonding in metals and compounds, which also relates to the ductility, could be described by the Cauchy pressure $C_{12}$–$C_{44}$. For metallic bonding the Cauchy pressure is typically positive. On the other hand, for directional bonding with angular character, the Cauchy pressure is negative, with larger negative pressure representing a more directional character. These correlations have been verified for ductile materials such as Ni and Al that have typical metallic bonding, as well as for brittle semiconductors such as Si with directional bonding [31]. In the $CsCdF_3$ compound, the calculated Cauchy pressure is 22.34 GPa within LDA and 14.83 GPa within GGA, in good agreement with the metallic characteristics of $CsCdF_3$ [32].

The calculated bulk modulus value from elastic constants has nearly the same one obtained from the EOS fitting. This may be an estimate of the reliability and accuracy of our calculated elastic constants. The dependence of the elastic constants on pressure assumes particular structural stability. The variation of the elastic moduli as a function of pressure is displayed in Figure 1. We observe that all these parameters increase monotonically and linearly with increasing pressure. We can notice that the increase in $C_{44}$ is weaker. For a cubic crystal under pressure $P$, the generalized elastic stability criteria [33,34] are:

$$\left\{\begin{array}{l}\frac{1}{3}(C_{11}+2C_{12}+P)>0\\(C_{44}-P)>0\\\frac{1}{2}(C_{11}-C_{12}-2P)>0\end{array}\right\}. \quad (1)$$

These criteria are satisfied in the studied pressure range, suggesting that the pure cubic $CsCdF_3$ is very stable under high compression.

From the theoretical elastic constants, we have computed the elastic wave velocities. The single-crystal elastic wave velocities in different directions are given by the resolution of the Christoffel equation [35]:

$$(C_{ijkl}n_jn_k-\rho v^2\delta_{il})u_l=0 \quad (2)$$

$C_{ijkl}$, $n$, $\rho$, $u$ and $v$ are the single-crystal elastic constant tensor, the wave propagation direction, the density of material, the wave polarization and the wave velocity. The solutions of this equation are of two types: a longitudinal wave with polarization parallel to the direction of propagation ($v_L$) and two shear waves ($v_{T1}$ and $v_{T2}$) with polarization perpendicular to $n$. The calculated elastic wave velocities along [100], [110] and [111] directions are listed in Table 3. Longitudinal and shear waves calculated within GGA and LDA are fastest along [100] and slowest along [100] and [110].

The main isotropic mechanical parameters for the cubic $CsCdF_3$, namely shear modulus $G$, Young's modulus $E$, Poisson's ratio $\sigma$, Lamé's constants ($\lambda$ and $\mu$) and $B/G$ ratio which are the important elastic moduli for applications, are calculated from the elastic constants of the single-crystals. Table 4 gives the calculated values of the mentioned elastic moduli for polycrystalline $CsCdF_3$ aggregate.

**Table 3.** Elastic wave velocities (in m/s) for different propagation directions for $CsCdF_3$ compound.

| | 100 | | | 110 | | | 111 | | |
|---|---|---|---|---|---|---|---|---|---|
| | $v_l$ | $v_{T1}$ | $v_{T2}$ | $v_L$ | $v_{T1}$ | $v_{T2}$ | $v_L$ | $v_{T1}$ | $v_{T2}$ |
| LDA | 4822 | 1926 | 1926 | 4370 | 3967 | 1926 | 4208 | 2546 | 2546 |
| GGA | 4270 | 1968 | 1968 | 4040 | 3400 | 1968 | 3961 | 2268 | 2268 |

**Table 4.** Calculated shear modulus $G$, Young's modulus $E$, Poisson's ratio $\sigma$ and Lamé's constants ($\lambda$ and $\mu$) and $B/G$ for polycrystalline $CsCdF_3$ compound.

| | $G$ | $E$ | $\sigma$ | $\lambda$ | $\mu$ | $B/G$ |
|---|---|---|---|---|---|---|
| LDA | 29.57 | 78.41 | 0.32 | 55.18 | 29.57 | 2.53 |
| GGA | 24.10 | 63.22 | 0.31 | 39.70 | 24.10 | 2.08 |

### 3.3 Debye temperature

The Debye temperature is an important fundamental parameter closely related to many physical properties such

**Table 5.** Calculated density $\rho$ (in g/cm$^3$), longitudinal, transverse and average sound velocity ($\upsilon_l$, $\upsilon_t$ and $\upsilon_m$, respectively, in m/s), calculated from polycrystalline elastic moduli, and Debye temperature ($\theta_D$ in K), calculated from the average sound velocity.

| | $\rho$ | $\upsilon_l$ | $\upsilon_t$ | $\upsilon_m$ | $\Theta_D$ |
|---|---|---|---|---|---|
| LDA | 5.8680 | 4414 | 2245 | 2516 | 306 |
| GGA | 5.2991 | 4073 | 2133 | 2385 | 280 |

as specific heat and melting temperature. At low temperature, the vibrational excitations arise solely from acoustic vibrations. Hence, at low temperature, Debye temperature calculated from elastic constants is the same as that determined from specific heat measurements. One of the standard methods to calculate Debye temperature $\theta_D$ is from elastic constants data, since $\theta_D$ may be estimated from the average sound velocity, $\upsilon_m$, by the following equation [36]:

$$\theta_D = \frac{h}{k_B}\left[\frac{3}{4\pi V_a}\right]^{\frac{1}{3}} \upsilon_m \tag{3}$$

where $h$, $k_B$ and $V_a$ are the Planck's constant, the Boltzmann's constant and the average atomic volume. The average sound velocity in the polycrystalline material is given by [37]:

$$\upsilon_m = \left[\frac{1}{3}\left(\frac{2}{\upsilon_t^3} + \frac{1}{\upsilon_l^3}\right)\right]^{-\frac{1}{3}} \tag{4}$$

where $\upsilon_l$ and $\upsilon_t$ are the longitudinal and transverse sound velocities in an isotropic material. These can be obtained from the shear modulus $G$ and the bulk modulus $B$, by the use of the Navier's equation [36]:

$$\upsilon_l = \left(\frac{3B + 4G}{3\rho}\right)^{\frac{1}{2}} \quad \text{and} \quad \upsilon_t = \left(\frac{G}{\rho}\right)^{\frac{1}{2}}. \tag{5}$$

The calculated sound velocities and Debye temperature as well as the density of $CsCdF_3$ are given in Table 5. Unfortunately, as far as we know, there are no data available in the literature on these properties for this compound. Future experimental work will test our calculated results. The average wave velocities in $CsCdF_3$ are smaller compared with those of $KMgF_3$.

### 3.4 Electronic properties

The calculated energy band structure for the equilibrium geometry of $CsCdF_3$ along the higher symmetry directions in the Brillouin zone is shown in Figure 2. The zero of energy is chosen to coincide with the valence band maximum (VBM), which occurs at R point, while the conduction band minimum (CBM) occurs at Γ point; thus, $CsCdF_3$ compound is an indirect energy band gap insulator. Calculated values of the main direct and indirect band gaps at zero pressure are given in Table 6. It is well known that the LDA and GGA calculations underestimate the fundamental gap of semiconductors and insulators; so

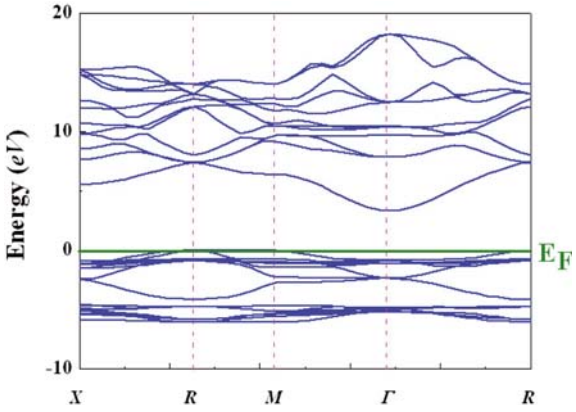


**Fig. 2.** (Color online) Band structure of $CsCdF_3$. The Fermi level is located at 0 eV.

**Table 6.** The calculated Γ-R, X-R, M-R and R-R gap energies and their first- and second-order pressure coefficients $\alpha$ (eV/GPa) and $\beta$ (eV/GPa$^2$).

| | | Γ-R | X-R | M-R | R-R |
|---|---|---|---|---|---|
| $E_g(0)$ | | | | | |
| | LDA | 3.14 | 5.77 | 6.45 | 6.97 |
| | GGA | 3.34 | 5.57 | 6.40 | 7.48 |
| $\alpha$ | | | | | |
| | LDA | 0.02 | 0.05 | 0.02 | –0.02 |
| | GGA | 0.03 | 0.06 | 0.04 | –0.02 |
| $\beta$ | | | | | |
| | LDA | –1.64 | –5.0 | –3.28 | 0.9 |
| | GGA | –3.00 | –6.5 | –6.5 | 0.7 |

our calculated band gap at equilibrium 3.34 eV (3.14 eV) using GGA (LDA) are in good agreement compared to those given by Vaitheeswarn et al. [7] 3.67 eV (3.16 eV). However, the underestimation of the gap between the valence and conduction bands is accurately calculated in the GGA (LDA) and do not depends on the type of functional form of the exchange-correlation potential [38]. To this end, the variation of main direct and indirect energy band gaps of $CsCdF_3$ as a function of pressure is plotted in Figure 3. As one can see, that all band-gaps have an increase quadratic when the pressure is enhanced except R-R, which decreases linearly. However, the Γ-R fundamental gap in $KMgH_3$ increases almost linearly with compression [28]. These curves correspond to the best fit of the energy gap-pressure data to the following expression:

$$E_g(P) = E_g(0) + \alpha P + \beta P^2 \tag{6}$$

$E_g$ is the energy gap, $P$ is the pressure, and $\alpha$ and $\beta$ are the first- and second-order pressure derivatives, respectively. The calculated values of $\alpha$ and $\beta$ for the studied band gaps of $CsCdF_3$ are given in Table 6. One can notice that band gaps calculated by GGA are slightly sensitive to pressure than those computed by LDA. As we know, there are no data available in the literature on the experiment gap value.

The calculated atomic site-projected $l$-decomposed densities of states (PDOS) of this compound are displayed

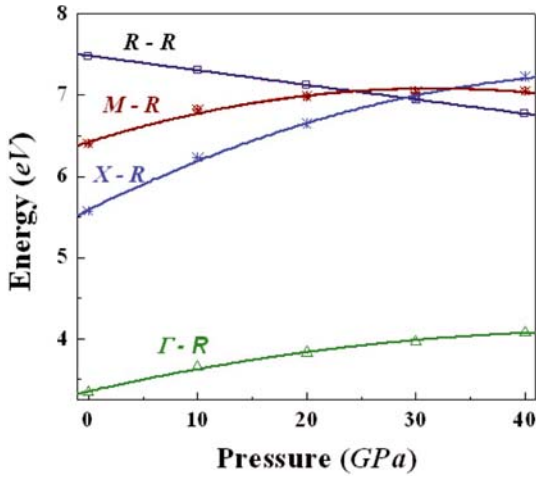


**Fig. 3.** (Color online) Direct R-R and indirect M-R, X-R and Γ-R band gap energies as a function of pressure.

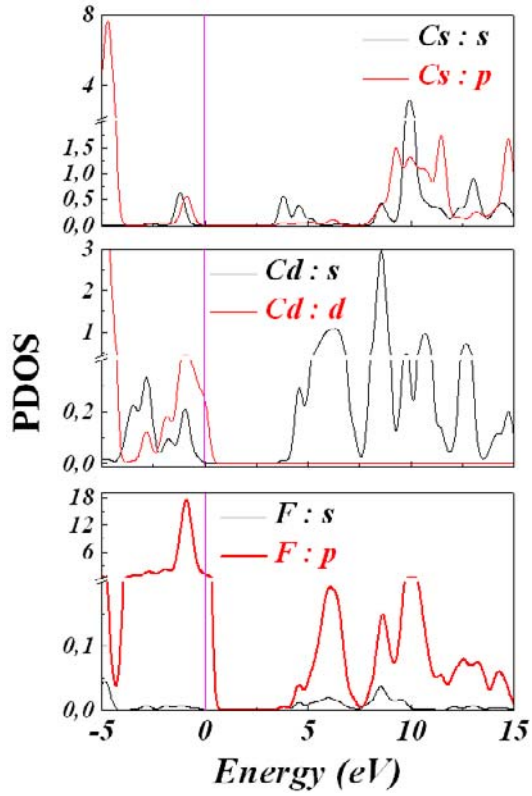


**Fig. 4.** (Color online) Calculated partial density of states (PDOS) of $CsCdF_3$.

in Figure 4. From the PDOS we are able to identify the angular momentum character of the different structures. The examination of PDOS reveals that the upper valence bands are dominantly consisted of F–$p$ states; there are small contribution from Cs–$p$ and Cd–$d$ states. There is hybridization between Cd–$d$ and F–$p$ states. The top of the valence band reflects the $p$ electronic character. The first conduction bands is mainly Cd–$s$ and Cs–$s$. This demonstrates that valence electrons are transferred from Cd or Cs sites to F sites [39].

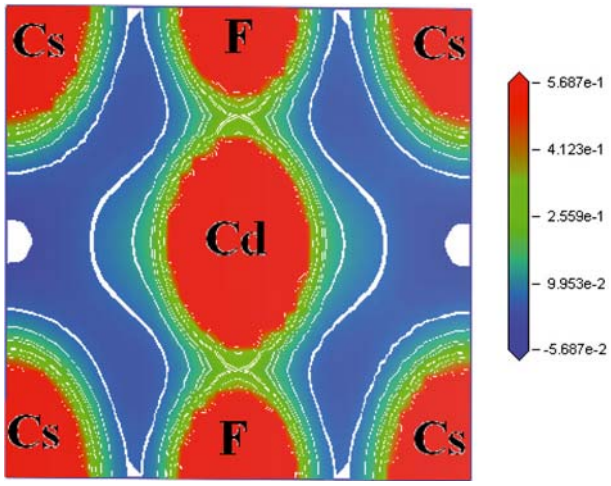


**Fig. 5.** (Color online) Valence charge density plots for the cubic perovskite-type $CsCdF_3$ in the (110) plane.

Figure 5 shows the charge density contour in the (110) plane for cubic perovskite $CsCdF_3$. Charge density maps serve as a complementary tool for achieving a proper understanding of the electronic structure of the system being studied. One can see that the highest charge density resides in the immediate vicinity of the nuclei. The near spherical charge distribution around the Cs indicates that the bonding between Cs and F is predominantly ionic. The figure reveals a sharing of charge between Cd and F due to the Cd–$d$ and F–$p$ hybridization; thus, there is a mixture of covalent-ionic bonding between Cd and F.

### 3.5 Optical properties

We display the real ($\varepsilon_1$) and imaginary ($\varepsilon_2$) parts of the dielectric function at zero pressure as a function of photon energy in Figure 6. The identification of interband transitions responsible for the structures of $\varepsilon_2$ requires the use of the band structure. The threshold energy of the dielectric function occurs at $E_0 = 3.29$ eV, which corresponds to the fundamental gap at equilibrium. The main peaks in the spectra are located at $E_1 = 6.46$ eV and $E_2 = 9.35$ eV, which correspond to the transition from the occupied state F–$p$ (valence band) to the unoccupied states Cd–$s$ and Cs–$s$ (conduction band) [40]. The first peak coincides with the M-R transition. For the interpretation of the optical spectra, it seems not realistic to attribute the transitions only to the present peaks in spectra, because many transitions can be observed in the band structure with an energy corresponding to the same peak. The static dielectric constant $\varepsilon_1(0)$ is 2.029. The computed refractive index and extinction coefficient spectrum are displayed in Figure 7. The static refractive index is found to have the value 1.42 and it increases with energy in the transparency region reaching a peak in the ultra violet at about 5.38 eV. All peaks of the refractive index and extinction coefficient coincide with a slightly shift.

The calculated linear absorption ($\alpha$) and the real part of conductivity ($\sigma$) in ($\Omega^{-1}$ cm$^{-1}$) spectrum of the optical

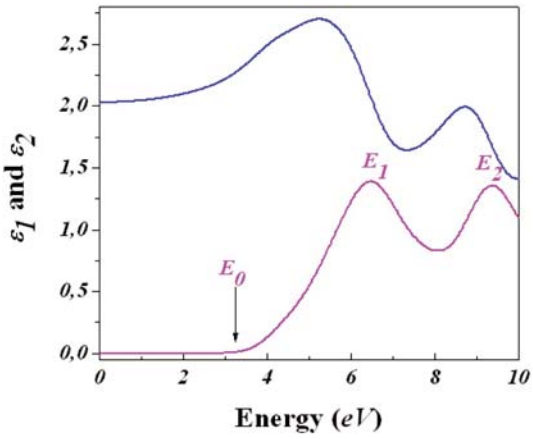


**Fig. 6.** (Color online) Real and imaginary part $\varepsilon_1$ and $\varepsilon_2$ of the dielectric function as a function of photon energy.

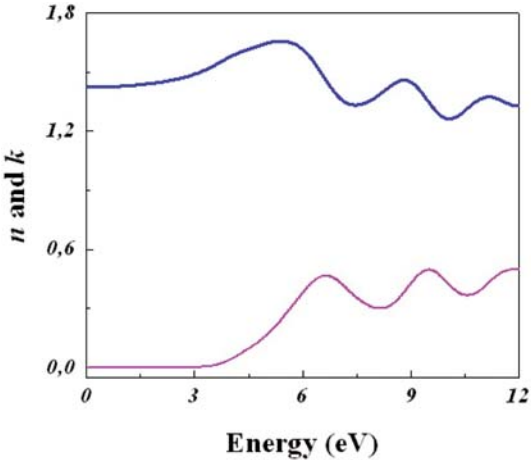


**Fig. 7.** (Color online) Refractive index and extinction coefficient as a function of photon energy.

conductivity of our compound are displayed in Figure 8. One can see that all details and peaks of the real part of the optical conductivity coincide with peaks of the absorption spectrum in the considered photon energy range. Probably, the optical conductivity in this compound is due mainly to the absorption in the high symmetry points in the first Brillouin zone. The absorption and conductivity edge start at 2.23 eV and their maximum are located at 14.95 eV.

Figure 9 shows the variation of the static dielectric constant and static refractive index within GGA and LDA as a function of pressure. These parameters increase monotonically with increasing pressure. We remark that the static dielectric constant and the static refractive index are proportional to the fundamental indirect band gap Γ-R. The pressure dependence of the static dielectric constant and static refractive index were determined by quadratic

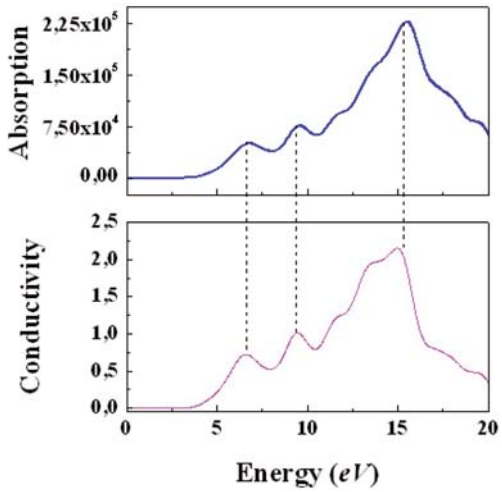


**Fig. 8.** (Color online) The calculated linear absorption and real part of the optical conductivity as a function of photon energy.

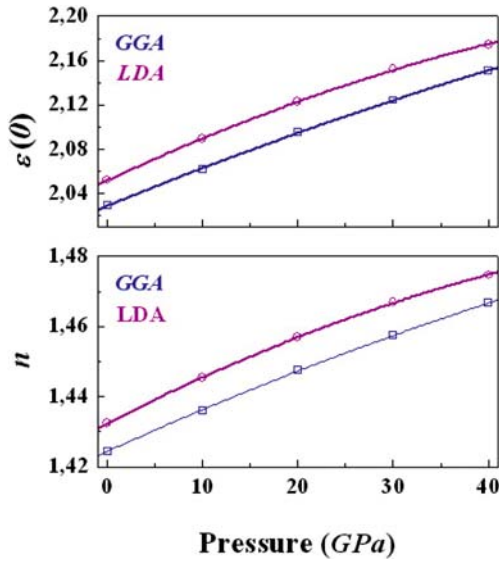


**Fig. 9.** (Color online) The static dielectric constant and static refractive index as a function of pressure within GGA and LDA.

polynomial fit giving the following relations:

$$\text{GGA}\left\{\begin{array}{l}\varepsilon_1 = 2.03 + 0.0035P - 1.14\times10^{-5}P^2\\ n = 1.424 + 0.001P - 4.3\times10^{-6}P^2\end{array}\right\} \quad (7)$$

$$\text{LDA}\left\{\begin{array}{l}\varepsilon_1 = 2.05 + 0.004P - 2.33\times10^{-5}P^2\\ n = 1.432 + 0.001P - 8.4\times10^{-6}P^2\end{array}\right\}. \quad (8)$$

### 3.6 Thermal properties

To investigate the thermal properties of $CsCdF_3$ compound under high temperature and high pressure, we have applied the quasi-harmonic Debye approximation. As a first step, a set of total energy calculation versus primitive cell volume ($E$-$V$), in the static approximation, was

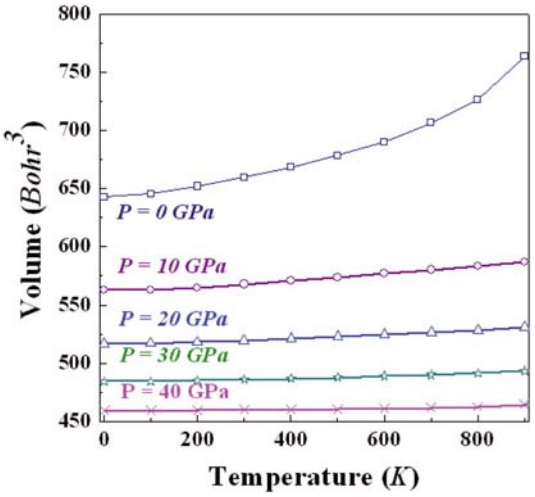


**Fig. 10.** (Color online) Variation of the volume as a function of temperature.

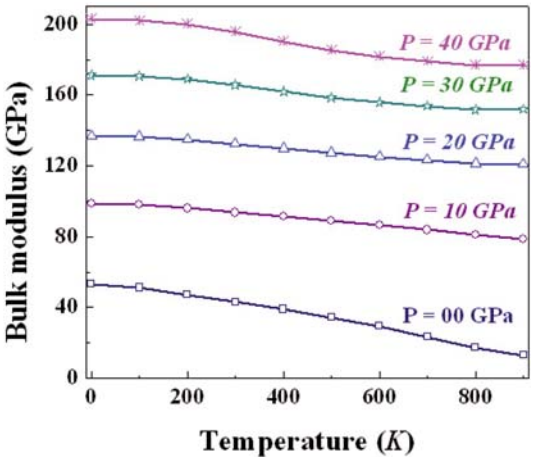


**Fig. 11.** (Color online) Variation of the bulk modulus as a function of temperature.

carried out and fitted with a numerical EOS in order to determine its structural parameters at $P = 0$ and $T = 0$, and then derive the macroscopic properties as function of $P$ and $T$ from standard thermodynamic relations. The thermal properties are determined in the temperature range from 0 to 900 K, where the quasi-harmonic model remains fully valid. The pressure effect is studied in the 0–40 GPa range.

In Figure 10, we present the volume-temperature diagram at several pressures. The volume increases linearly with increasing temperature, except at equilibrium, where the variation is quadratic. On the other side, as the pressure $P$ increases the volume decreases at a given temperature. The rate of increase in volume with temperature decreases with increasing pressure.

Figures 11 and 12 show respectively the variation of bulk modulus and Debye temperature versus temperature at a various pressure. One can notice that the bulk modulus and Debye temperature are nearly constant from 0 to 100 K and then decrease with increasing temperature.

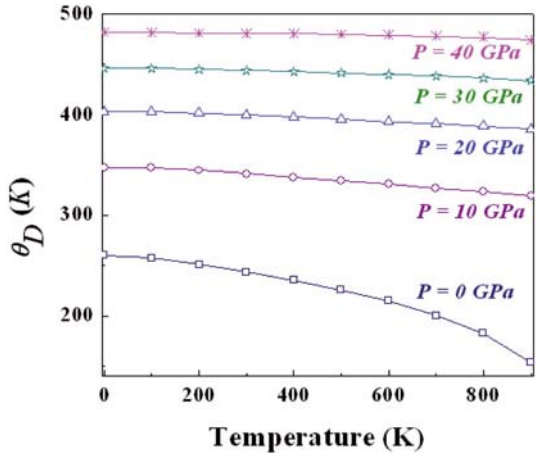


**Fig. 12.** (Color online) Variation of Debye temperature as a function of temperature.

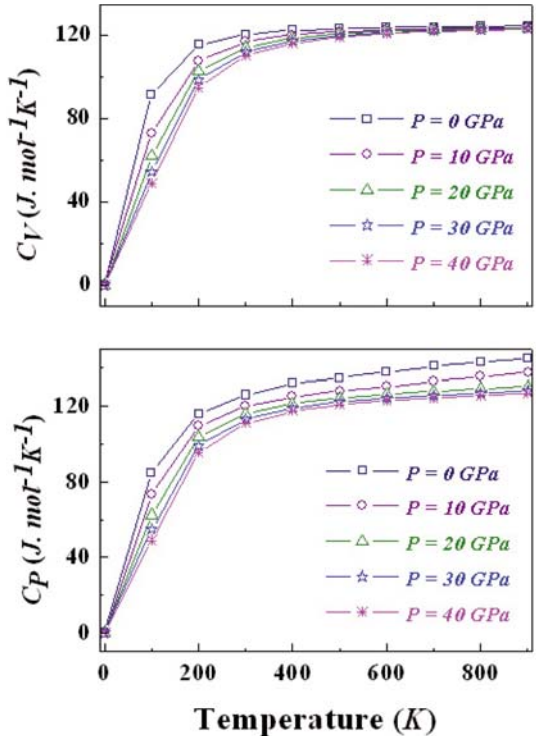


**Fig. 13.** (Color online) Variation of the heat capacities $C_V$ and $C_P$ versus temperature at various pressures.

They increase with increasing pressure at a given temperature. These results are due to the fact that the effect of increasing pressure on the material is the same as the decreasing temperature. Our calculated $\theta_D$ at zero pressure and ambient temperature is 243 K, which is in good agreement with the value of 280 K computed accurately in terms of the elastic constants (Tab. 5). This might be an indication that the quasi-harmonic Debye model is a very reasonable alternative to account for the thermal effects with no expensive task in terms of computational time.

The knowledge of the heat capacity of a substance provides essential insight into its vibrational properties and is also mandatory for many applications. Two famous

limiting cases are correctly predicted by the standard elastic continuum theory [41]. At high temperature, the constant volume heat capacity $C_V$ tends to the Dulong-Petit limit [42]. At sufficiently low temperature, $C_V$ is proportional to $T^3$ [41]. At intermediate temperatures, the dependence of $C_V$ on temperature is governed by the details of vibrations of the atoms and for a long time could only be determined from experiments. Figure 13 represents the variation of the heat capacities $C_V$ and $C_P$ as a function of temperature for various pressures. It is shown that when $T < 500$ K, $C_V$ and $C_P$ are depending on both temperature and pressure and increase exponentially. When the temperature is constant, $C_V$ and $C_P$ decrease with the applied pressures. At high temperature ($T > 500$ K), $C_V$ and $C_P$ tend to the Dulong-Petit limit and a linear increase respectively. At high temperature $C_V$ tends to approach 123 J mol$^{-1}$ K$^{-1}$. At zero pressure and 300 K, $C_V$ and $C_P$ are 120.7 and 126 J mol$^{-1}$ K$^{-1}$.

## 4 Conclusion

The ideal perovskite $CsCdF_3$ was studied using the PP-PW method based on the density functional theory with both LDA and GGA. A linear pressure dependence of the elastic stiffnesses and bulk modulus were found. A set of isotropic parameters (bulk modulus, shear modulus, Young's modulus, Poisson's ration, average sound velocity and Debye temperature) are estimated for ideal polycrystalline $CsCdF_3$ aggregate. The analysis of the PDOS and charge density reveals that bonds between the constituting elements of this compound are mainly ionic. Through the quasi-harmonic Debye model, the dependences of the volume, bulk modulus, heat capacities and Debye temperature on temperature and pressure have been obtained successfully. To the author's knowledge, most of the studied properties are reported for the first time.

## References


1. R. Hua, B. Lei, D. Xie, C. Shi, J. Solid State Chem. **175**, 284 (2003)
2. K. Shimamura, H. Sato, A. Bensalah, V. Sudesh, H. Machida, N. Sarukura, T. Fukuda, Cryst. Res. Technol. **36**, 801 (2001)
3. P. Berastegui, S. Hull, S.-G. Eriksson, J. Phys.: Condens. Matter **13**, 5077 (2001)
4. J. Julliard, J. Nouet, Rev. Phys. Appl. **10**, 325 (1975)
5. R.R. Daniels, G. Margaritondo, R.A. Heaton, C.C. Lin, Phys. Rev. B **27**, 3878 (1983)
6. A.S. Verma, V.K. Jindal, J. Alloys Compd. **485**, 514 (2009)
7. G. Vaitheeswaran, V. Kanchana, R.S. Kumar, A.L. Cornelius, M.F. Nicol, A. Svane, N.E. Christensen, O. Eriksson, Phys. Rev. B **81**, 075105 (2010)
8. J. Tong, C. Lee, M.-H. Whangbo, R.K. Kremer, A. Simon, J. Köhler, Solid State Sci. **12**, 680 (2010)
9. B. Ghebouli, M.A. Ghebouli, M. Fatmi, A. Bouhemadou, Solid State Commun. **150**, 1896 (2010)
10. M.W. Lufaso, P.M. Woodward, Acta Cryst. B **57**, 725 (2001)
11. P. Goudochnikov, A.J. Bell, J. Phys.: Condens. Matter **19**, 176201 (2007)
12. C. Li, B. Wang, R. Wang, H. Wang, X. Lu, Physica B **403**, 539 (2008)
13. M.D. Segall, P.J.D. Lindan, M.J. Probert, C.J. Pickard, P.J. Hasnip, S.J. Clark, M.C. Payne, J. Phys.: Condens. Matter **14**, 2717 (2002)
14. D. Vanderbilt, Phys. Rev. B **41**, 7892 (1990)
15. D.M. Ceperly, B.J. Alder, Phys. Rev. Lett. **45**, 566 (1980)
16. J.P. Perdew, A. Zunger, Phys. Rev. B **23**, 5048 (1981)
17. J.P. Perdew, K. Burke, M. Ernzerhof, Phys. Rev. Lett. **77**, 3865 (1996)
18. H.J. Monkhorst, J.D. Pack, Phys. Rev. B **13**, 5188 (1976)
19. B.G. Pfrommer, M. Côté, S.G. Louie, M.L. Cohen, J. Comput. Phys. **131**, 233 (1997)
20. M.A. Blanco, E. Francisco, V. Luaña, Comput. Phys. Commun. **158**, 57 (2004)
21. M.A. Blanco, A.M. Pendás, E. Francisco, J.M. Recio, R. Franco, J. Mol. Struct. Theochem. **368**, 245 (1996)
22. M. Flórez, J.M. Recio, E. Francisco, M.A. Blanco, A.M. Pendás, Phys. Rev. B **66**, 144112 (2002)
23. E. Francisco, J.M. Recio, M.A. Blanco, A.M. Pendás, J. Phys. Chem. **102**, 1595 (1998)
24. E. Francisco, M.A. Blanco, G. Sanjurjo, Phys. Rev. B **63**, 049107 (2001)
25. R.L. Moreira, A. Dias, J. Phys. Chem. Solids **68**, 1617 (2007)
26. L.Q. Jiang, J.K. Guo, H.B. Liu, M. Zhu, X. Zhou, P. Wu, C.H. Li, J. Phys. Chem. Solids **67**, 1531 (2006)
27. F.D. Murnaghan, Proc. Natl. Acad. Sci. USA **30**, 244 (1994)
28. G. Vaitheeswaran, V. Kanchana, R.S. Kumar, A.L. Cornelius, M.F. Nicol, A. Svane, A. Delin, B. Johansson, Phys. Rev. B **76**, 014107 (2007)
29. M. Rousseau, J.Y. Gesland, J. Julliard, J. Nouet, J. Zarembowitch, A. Zarembowitch, Phys. Rev. B **12**, 1579 (1975)
30. S.F. Pugh, Philos. Mag. **45**, 823 (1954)
31. D. Pettifor, Mater. Sci. Technol. **8**, 345 (1992)
32. V. Kanchana, G. Vaitheeswaran, A. Svane, A. Delin, J. Phys.: Condens. Matter **18**, 9615 (2006)
33. S. Yip, J. Li, M. Tang, J. Wang, Mater. Sci. Eng. A **317**, 236 (2001)
34. G.V. Sin'ko, N.A. Smimov, J. Phys.: Condens. Matter **14**, 6989 (2002)
35. B.B. Karki, L. Stixrude, S.J. Clark, M.C. Warren, G.J. Ackland, J. Crain, Am. Mineral. **82**, 51 (1997)
36. O.L. Anderson, J. Phys. Chem. Solids **24**, 909 (1963)
37. E. Schreiber, O.L. Anderson, N. Soga, *Elastic Constants and Their Measurements* (McGraw-Hill, New York, 1973)
38. S. Fahy, K.J. Chang, S.G. Louie, M.L. Cohen, Phys. Rev. B **35**, 5856 (1987)
39. P. Vajeeston, P. Ravindran, A. Kjekshus, H. Fjellvåg, J. Alloys Compd. **450**, 327 (2008)
40. R.D. King-Smith, D. Vanderbilt, Phys. Rev. B **47**, 1651 (1992)
41. P. Debye, Ann. Phys. **39**, 789 (1912)
42. A.T. Petit, P.L. Dulong, Ann. Chim. Phys. **10**, 395 (1819)